Title: Sustained systemic hyaluronan in COVID-19 patients, a 3D-lung model reveals mechanisms of overproduction counteracted by cortisone

Urban Hellman[1,2], Ebba Rosendal[1,3], Alicia Edin[4], Johan Henriksson[3,5], Mattias N.E. Forsell[1], Anna Lange[6], Clas Ahlm[1], Anders Blomberg[2], Sara Cajander[6], Johan Normark[1,7], Anna K Överby[1,3*], Annasara Lenman[1*]

[1]Department of Clinical Microbiology, Umeå University, Umeå, Sweden

[2]Department of Public Health and Clinical Medicine, Umeå University, Umeå, Sweden

[3]The laboratory for Molecular Infection Medicine Sweden (MIMS), Umeå University, Umeå, Sweden

[4] Department of Surgical and Perioperative Sciences, Umeå University, Umeå, Sweden.

[5]Department of Molecular Biology and Umeå Centre for Microbial Research (UCMR), Umeå University, Umeå, Sweden

[6]Department of Infectious diseases, Faculty of Medicine and Health, Örebro University, Örebro, Sweden.

[7]Wallenberg Centre for Molecular Medicine, Umeå University, Sweden

[*]*These authors contributed equally*

Correspondence and requests for reprints should be addressed to Ph.D. Annasara Lenman, Department of Clinical Microbiology, Umeå University, Umeå, Sweden. Email: annasara.lenman@umu.se

Author contributions: A.L., E.R., C.A., A.B., A.K.Ö and U.H. designed the study. A.L., E.R. and U.H. conducted experiments and analyzed the results. A.E., L.D., A.La., M.F., S.C. and J.N. performed inclusion and sampling of patients, collected, managed, and analyzed clinical data. J.H. analyzed transcriptomics data. A.L., A.E, C.A., A.B., A.K.Ö., and U.H. wrote the manuscript with input from all authors.

This study was supported by: the Swedish Heart-Lung Foundation (20200385 to A.K.Ö & A.L., 20200325 & 20210078 to C.A., and 20200366 & 20210049 to A.B.), SciLife Lab COVID-19 research program funded by the Knut and Alice Wallenberg Foundation (2020.0182 & C19R:028 to A.K.Ö. & A.L., and VC-2020-0015 to C.A.), Kempestiftelserna (grant no. JCK-1827 to A.K.Ö.), Umeå University and County Council of Västerbotten (#RV-938855 to C.A. and #RV-970074 to A.K.Ö.), Carl Bennet AB (A.L.), the Fundraising Foundation for Medical Research, Umeå University (978018 to A.L. and 964781 to U.H.), Nyckelfonden Örebro (OLL-938628, OLL-961416 to S.C.), Regional Research Council Mid Sweden (RFR-968856, RFR-940474 to S.C), the Swedish Research Council (2020-06235 to M.N.E.F, 2016-06514 to J.N., 2021-06602 to J.H.), J.N. is a Wallenberg Centre for Molecular Medicine Associated Researcher. Computations were performed using resources provided by SNIC through Uppsala Multidisciplinary Center for Advanced Computational Science (UPPMAX) under Project SNIC 2021/22-697 to J.H. Apart from funding, the sponsors were not involved in performing the present study.

ABSTRACT

Rationale: High levels of hyaluronan in lungs and blood associate with COVID-19 severity. However, the effects on systemic hyaluronan concentrations and the mechanisms involved in the pathological overproduction of hyaluronan upon SARS-CoV-2 infection remain incompletely characterized.

Objectives: To determine how hyaluronan levels in blood of COVID-19 patients change over time and investigate SARS-CoV-2 impact on hyaluronan metabolism along with the effect of corticosteroid treatment.

Methods: The concentrations of hyaluronan were measured in blood plasma from patients with mild (WHO Clinical Progression Scale, WHO-CPS, 1-5) and severe COVID-19 (WHO-CPS 6-9), both during the acute and convalescent phases. Primary human bronchial epithelial cells isolated from healthy donors were differentiated into an *in vitro* 3D-lung model and used to study effects of SARS-CoV-2 infection and corticosteroids treatment on hyaluronan metabolism.

Measurements and Main results: Compared to healthy controls, both patients with mild and severe COVID-19 showed elevated plasma hyaluronan concentrations, which increased with disease severity. A reduction was observed over time, but hyaluronan levels remained elevated for at least 12 weeks, especially in women. SARS-CoV-2 infection in the 3D-lung model showed upregulation of inflammatory genes, hyaluronan synthases and downregulation of hyaluronidases, which increased the overall hyaluronan concentration. Notably, several of these effects were counteracted by corticosteroid treatment.

Conclusions: Overproduction of hyaluronan plays a role in the pathogenesis of COVID-19 and hyaluronan levels in blood remain elevated over time. The *in vitro* mechanism for the positive effects of corticosteroid treatment in COVID-19 suggests a combined action of reduced inflammation and counteraction of hyaluronan synthesis.

INTRODUCTION

The ongoing pandemic caused by severe acute respiratory syndrome coronavirus 2 (SARS-CoV-2) has hitherto caused more than 6.5 million reported deaths globally (by October 31, 2022, according to WHO). The clinical manifestations of COVID-19 ranges from asymptomatic or mild disease with symptoms from the upper respiratory tract to severe pneumonitis with acute respiratory distress syndrome (ARDS) and multiorgan failure. Several pathophysiological mechanisms have been described as contributing to respiratory failure in COVID-19, including hyperinflammation with disturbed coagulation, leading to disseminated pulmonary microthrombi as well as diffuse alveolar damage, alveolar septal fibrous proliferation and pulmonary consolidation (1, 2).

Hyaluronan (HA) is a glycosaminoglycan that constitutes an important structural component of the extracellular matrix in tissues. Through interactions with cell-surface receptors, HA also regulates cellular functions, such as cell-matrix signaling, cell proliferation, angiogenesis and cell migration (3). In addition, HA has a very high water-binding capacity, with the ability to occupy a large hydrated volume up to 1,000 times its molecular mass, which can promote edema formation (3). Accumulation of HA is associated with ARDS (4), and recent publications have shown increased levels of HA in the lungs of deceased COVID-19 patients (5, 6) as well as elevated plasma levels of HA in severe cases (7, 8). Anti-inflammatory treatment with the corticosteroid dexamethasone results in lower mortality amongst hospitalized COVID-19 patients (9). Corticosteroids are known to be effective in reducing HA levels in other inflammatory syndromes (10, 11), thus, clearance of HA may be critical in disease resolution following COVID-19 (5).

With an increasing number of reports implying the involvement of HA in severe COVID-19 disease, there is a need to better understand the molecular mechanisms involved in pathological overproduction of HA in severe COVID-19, and how steroid treatment may be beneficial. The aims of the present study were to determine HA concentration in peripheral blood of patients with COVID-19, and to correlate HA levels during the acute and convalescent phases to severity of disease, age and sex. In addition, we established an *in vitro* 3D-lung model to investigate the effects on HA metabolism in SARS-CoV-2 infection as well as the impact of corticosteroid treatment.

METHODS

Study design and study population

Data and clinical samples were obtained from the CoVUm study, a prospective, multicenter observational study of COVID-19 including patients from Umeå and Örebro, and coordinated from Umeå University, Sweden (www.clinicaltrials.gov identifier NCT 04368013). Non-hospitalized patients aged ≥15 years and hospitalized patients aged ≥18 years with a positive PCR-test for SARS-CoV-2 were enrolled in the study. Written informed consent was obtained from all participants or their next of kin before the first sampling timepoint. Blood samples were obtained at acute phase (0-4 weeks after onset) and convalescent phase (≥12 weeks). For study outline, see Figure 1A. Participants were classified as “severe” if they required high-flow nasal oxygen treatment (HFNO) and/or was admitted to the intensive care unit (ICU) during the acute phase of illness, corresponding to WHO Clinical Progression Scale (WHO-CPS) 6-9 (12). All other participants were classified as “mild”, corresponding to WHO-CPS 1-5. A healthy control group, consisting of plasma samples collected from anonymous blood donors was included for reference. The study was performed according to the Declaration of Helsinki and approved by the Swedish Ethical Review Authority.

Data collection and clinical samples

All clinical metadata including: age, sex, level of education, Charlson Comorbidity Index (CCI) (13), medication at enrollment, body mass index, symptom assessment, vital signs, type of respiratory support and medical treatment were collected and managed using the REDCap electronic data capture tools hosted at Umeå University (14, 15). Clinical chemistry data of conventional inflammatory markers were extracted retrospectively from the patients' electronic medical records. The highest and lowest values of each biomarker from each individual, during the first 180 days after symptom onset were extracted for further analysis. Plasma samples used for HA analysis were collected at each timepoint in 6 ml EDTA tubes (BD Diagnostics).

Measurement of hyaluronan concentration in plasma samples

Plasma hyaluronan (HA) concentrations were measured with a competitive HA-binding protein-based enzyme-linked immunosorbent assay (ELISA)-like concentration measurement kit (K-1200; Echelon Biosciences Inc., Salt Lake City, UT, USA), according to the manufacturer's instructions. Samples were run in duplicate and a coefficient of variation (CV) < 10% was considered acceptable. Absorbance was measured on a ThermoMultiskan Ascent (Thermo Fisher Scientific, MA, USA) and plotted by polynomial regression against the concentration of the standard curve.

Assessment of hyaluronan metabolic pathways upon SARS-CoV-2 infection in an *in vitro* 3D-lung model

(i) Generation of the human primary 3D-lung model

Primary human bronchial epithelial cells (HBEC) were isolated from proximal airway tissue obtained with informed consent from two patients, who underwent thoracic surgery at the University Hospital, Umeå, Sweden (ethical permission approved by the Regional Swedish

Ethical Review Authority in Umeå). HBECs were grown and differentiated at an air-liquid interface (ALI) forming an *in vitro* 3D-lung model as previously described (16). In short, HBECs were grown and differentiated on 6.5 mm semipermeable transwell inserts (0.4 µm Pore Polyester Membrane Insert, Corning) and after two weeks at air-liquid interface (ALI) the cultures reached full differentiation, which was assessed using light microscopy focusing on epithelial morphology, presence of ciliated cells, and mucus production along with immunofluorescence staining for ciliated cells (acetylated-tubulin, T6793, Sigma) and goblet cells (muc5AC, Ab-1 (45M1), #MS-145-P, ThermoFisher).

(ii) Betamethasone treatment

Fully differentiated HBEC-ALI cultures were either mock treated or treated with betamethasone (Alfasigma) 20 h prior to infection by addition of 700 µl fresh basal media containing 0.3 µM betamethasone. For study outline see Figure 1B. Shortly before infection, the basal media was exchanged once more and betamethasone was replenished in the treated wells. Betamethasone was replenished every 24 h post infection.

(iii) SARS-CoV-2 infection

The clinical isolate SARS-CoV-2/01/human/2020/SWE (GeneBank accession no. MT093571.1) was kindly provided by the Public Health Agency of Sweden. Vero E6 cells were cultured in Dulbecco's modified Eagle's medium (DMEM, D5648 Sigma) supplemented with 5% FBS (HyClone), 100 U/mL penicillin and 100 µg/ml streptomycin (PeSt, HyClone) at 37°C in 5% CO_2. Propagation of the virus was done once in Vero E6 cells for 72 h and titration was done by plaque assay. The apical side of the HBEC ALI-cultures were rinsed three times with warm PBS shortly before infection. 1.5×10^4 plaque forming units (PFU) of SARS-CoV-2 was added to the apical compartment in a total volume of 100 µl infection medium (DMEM / PeSt), corresponding to an approximate multiplicity of infection (MOI) of 0.05. The HBEC ALI-

cultures were incubated at 37°C and 5% CO_2 for 2.5 h before the inoculum was removed and the cultures were washed with PBS to remove residual medium.

(iv) Sample collection

Accumulated progeny virus and secretions were collected from the apical side of the HBEC ALI-cultures every 24 h by addition of 100 µl warm PBS to the apical chamber followed by a 1 h incubation at 37°C and 5% CO_2. The collected samples were stored at –80°C until RNA extraction. The progression of the infection was monitored for four days (96 h post infection).

(iv) Virus quantification by qPCR

Viral RNA secreted from HBEC ALI-cultures was extracted from 50 µl of the apical samples using the QIAmp Viral RNA kit (Qiagen) following the manufacturer's instructions, and cDNA was synthesized from 10 µl of eluted RNA. RT-qPCR for SARS-CoV-2 RNA was performed in duplicates on a StepOnePlus™ Real-Time PCR System (Applied Biosystems) using the qPCRBIO Probe Mix Hi-ROX (PCR biosystems) and primers (Forward: GTCATGTGTGGCGGTTCACT, Reverse: CAACACTATTAGCATAAGCAGTTGT) and probe (CAGGTGGAACCTCATCAGGAGATGC) specific for viral RdRp.

Transcriptomics, total RNA sequencing

At 96 h post infection the mock treated (n=3), infected (n=3) and infected + betamethasone treated (n=3) HBEC ALI-cultures were washed three times on both sides with PBS. The HBEC ALI-cultures were then lysed and RNA extraction was done using the NucleoSpin RNA II kit (Macherey-Nagel) following the manufacturer's instructions. RNA-seq libraries were prepared using the Smart-seq2 method, and sequenced on an Illumina NextSeq 500 (75PE, v2.5 High Output kit). STAR 2.7.1a was used to align the reads against a reference genome consisting of GRCh38 and Sars_cov_2.ASM985889v3. A gene expression table was produced using featureCounts (17). Differential expression analysis was performed using DESeq2 (18).

Cytokine quantification

At 96 h post infection, samples were collected from the basal chambers of each of the HBEC ALI-cultures. The samples were inactivated with Triton X-100 at a final concentration of 1% followed by incubation at room temperature for 3 h. The levels of 45 cytokines were quantified by Proximity Extension Assay (Olink Target 48 Cytokine panel at Affinity Proteomics Uppsala, SciLifeLab Sweden), which gives absolute (pg/mL) and relative (normalized protein expression, NPX) concentration measurements of 45 pre-selected cytokines.

Quantification of HA synthases and hyaluronidases by qPCR

Total RNA from cells were extracted using the Nucleo-Spin RNA II kit (Macherey-Nagel). 1000 ng of RNA was used as input for cDNA synthesis using High-capacity cDNA Reverse Transcription kit (Thermo Fisher). Cellular HA synthases (*HAS1, 2* and *3*) and hyaluronidases (*HYAL1* and *2*) were quantified using qPCRBIO SyGreen mix Hi-ROX (PCR Biosystems) and QuantiTect primer assay (Qiagen, *HAS1*;QT02588509, *HAS2*;QT00027510, *HAS3*;QT00014903, *HYAL1*;QT01673413, *HYAL2*;QT00013363) with actin as a housekeeping gene (QT01680476) and run on a StepOnePlus^{TM} Real-Time PCR System (Applied Biosystems).

Measurement of HA concentration in apical secretions from HBEC ALI-cultures

Apical secretions from HBEC ALI-cultures were collected at 120 h post infection and HA concentrations were measured with a Hyaluronic Acid AlphaScreen Assay (K-5800; Echelon Biosciences Inc., Salt Lake City, UT, USA), according to the manufacturer's instructions. AlphaScreen beads from the Histidine (Nickel Chelate) Detection Kit (PerkinElmer, MA, USA) was used. Chemiluminescent emission was measured on a SpectraMax i3x (Molecular Devices, CA, USA) and plotted by polynomial regression against the concentration of the standard curve.

Statistical analysis

Statistical analysis was performed by using Prism 9 (Graphpad software) and Jamovi version 1.6 (The jamovi project (2021)). jamovi (Version 1.6) [Computer Software]. Retrieved from https://www.jamovi.org). Descriptive variables of the patient cohort were analyzed by Mann-Whitney U-test (continuous variables) and Fisher's exact test (dichotomous variables). No correction for multiple testing was performed.

Data availability

The CoVUm data cannot be made publicly available, according to Swedish data protection laws and the terms of ethical approval that were stipulated by the Ethical Review Authority of Sweden. Access to data from the CoVUm database is organised according to a strict data access procedure, to comply with Swedish law. For all types of access, a research proposal must be submitted to the corresponding authors for evaluation. After evaluation, data access is contingent on vetting by the Ethical Review Authority of Sweden, according to the Act (2003:460) concerning the Ethical Review of Research Involving Humans.

RESULTS

Study population

At data export on May 4, 2022, a total of 528 participants, enrolled between 27 April 2020 and 28 May 2021, had been registered in the CoVUm database. Seven of the participants were excluded since they did not fulfill the inclusion criteria (false positive PCR-tests for SARS-CoV-2). Out of the remaining 521 participants, all patients classified as severely ill during the acute phase of the disease, and with available blood samples, were selected for this study. These were matched to mild patients with respect to sex and age. In total 103 individuals were selected; 37 patients were classified as severe and 66 patients as mild. The demography and clinical characteristics are presented in Table 1. The groups differed significantly in BMI, minimum levels of hemoglobin, maximum levels of C-reactive protein, white blood cell count, and neutrophil count (Table 1). No significant differences were observed when it came to comorbidities at baseline. Thirty-two (86.5%) patients in the severe group and four (6.1%) in the mild group received corticosteroid treatment ($p < 0.001$). Most of these patients, 28 in the severe and two in the mild group, received the first dose before the first sampling timepoint.

Hyaluronan levels increase in severe COVID-19 and remain elevated into the convalescent phase

The concentration of HA in plasma samples was determined using ELISA in order to assess the involvement of HA in disease severity. A general increase in HA concentrations was observed in samples taken during the acute phase of the disease in both patients with mild and severe COVID-19, as compared to healthy controls (Figure 2A). The HA concentrations were even further increased in patients with severe COVID-19. Interestingly, although HA concentrations declined in the convalescent phase (mild $p < 0.0001$, severe $p < 0.0001$), they remained elevated compared to healthy controls, especially in the severe group. A sex comparison of HA plasma

concentrations in the acute phase showed a similar increase in HA in severe COVID-19 in women and men (Figure 2B). However, in the convalescent phase of mild COVID-19, the HA levels remained higher for women compared to men (p=0.043, data not shown). Analyses assessing the impact of age showed an increase in HA concentrations in severe compared to mild COVID-19 in both older (60-89 years) and younger (18-59 years) patients, with a general trend towards higher HA concentrations in the older age group (mild disease: p=0.01, severe disease: p=0.17) (Figure 2C). In summary, plasma concentrations of HA were substantially increased in COVID-19 patients and correlated to disease severity. To further study the potential mechanisms behind the increase in HA in COVID-19, we performed infection experiments in a human 3D-lung model.

SARS-CoV-2 infection causes an inflammatory response, which is counteracted by corticosteroids in a human 3D-lung model

We used a lung model that closely resembles the human respiratory tract based on primary human bronchial epithelial cells (HBECs) isolated from human donors. This model was used to characterize the cellular pathways affected by SARS-CoV-2 infection and the effects of corticosteroid treatment with respect to inflammation and HA metabolism. These cells were differentiated at an air-liquid interface (ALI) to form a polarized epithelium containing an apical layer of fully functional secretory and ciliated cells and an underlying layer of basal cells (16). The lung cultures were pretreated with, or without, the corticosteroid betamethasone, and then infected with SARS-CoV-2. The course of infection was monitored daily by collection of apical secretions containing released progeny virus and the viral load was quantified by qPCR. A distinct increase in viral RNA was observed over time, indicating an active viral replication in the HBEC ALI-cultures (Figure 3A). Betamethasone-treated cultures showed reduced levels of released progeny virus. The infected HBEC ALI-cultures were harvested at 96h post infection

and subjected to total RNA sequencing, to identify the mechanisms and pathways regulated by SARS-CoV-2 infection and betamethasone treatment. Statistical comparison of genes expressed in uninfected vs. infected HBEC ALI-cultures (Figure 3B, Supplementary Table 1) identified 167 differentially expressed genes (DEGs) that were upregulated upon SARS-CoV-2 infection, with a strong enrichment of genes involves in the immune response, especially type I interferon (IFN-I) signaling. A similar statistical comparison of infected HBEC ALI-cultures with or without betamethasone treatment was performed to evaluate the effect of betamethasone treatment. This identified 102 genes that were upregulated, and 229 genes that were downregulated in the betamethasone-treated cultures (Figure 3C, Supplementary Table 1). Interestingly, many of the 167 genes upregulated by infection (Figure 3B) were downregulated by betamethasone treatment (Figure 3C), as shown by the overlapping genes in a comparison of DEGs from the two groups (Figure 3D). A heatmap displaying the expression values of the individual overlapping genes showed a clear upregulation of these genes by SARS-CoV-2 infection, which was counteracted by betamethasone treatment (Figure 3E). Several of the affected genes were involved in inflammatory responses, correlating well with the anti-inflammatory activity of betamethasone. We also collected basolateral samples from the HBEC ALI-cultures at 96h post infection and analyzed these with a targeted cytokine panel based on proximity extension assay, allowing a quantitative concentration measurement of each cytokine (Figure 3F). Of the ten cytokines that showed significant changes, eight were downregulated by betamethasone treatment, but not affected by the infection. CXCL10 and CXCL11 were both upregulated by the SARS-CoV-2 infection and subsequently downregulated by steroid treatment.

SARS-CoV-2 affects HA metabolism by upregulation of HA synthases and downregulation of hyaluronidases

To further investigate the direct effect of SARS-CoV-2 on HA synthesis and degradation, expression levels of the three human hyaluronan synthases, *HAS1, HAS2* and *HAS3* and the two major hyaluronidases, *HYAL1* and *HYAL2*, were determined in HBEC ALI-cultures from two different donors five days post infection. No effect was seen on *HAS1* expression, but SARS-CoV-2 infection increased *HAS*2 in donor 2 and *HAS3* expression in both donors (Figure 4A-C). Betamethasone treatment of infected cultures resulted in a reduction of the upregulated *HAS2* expression in donor 2 and *HAS3* in donor 1 (Figure 4B, C). Additionally, SARS-CoV-2 infection decreased expression of hyaluronidase *HYAL1* in both donors and *HYAL2* in donor 2 (Figure 4D, E). The hyaluronidase genes were not significantly affected by betamethasone treatment (Figure 4D, E). Both upregulation of HA synthases and downregulation of degrading hyaluronidases can induce an increase of HA concentrations. Indeed, measurements of HA concentrations in the apical secretions from HBEC ALI-cultures confirmed the transcriptional changes with an increase in HA in cultures infected by SARS-CoV-2, which were kept at baseline concentrations when simultaneously treated with betamethasone (Figure 4F).

Taken together, our results identified a large number of genes involved in viral defense and inflammation affected by SARS-CoV-2 infection. Betamethasone treatment demonstrated a general counteraction against the viral transcriptional effect. SARS-CoV-2 infection and betamethasone treatment also affected a number of genes with potential impact on HA production and degradation. In addition to the effects on HA synthases and hyaluronidases, we observed an upregulation of transcription factors early growth response 1 and 2 (*EGR1, 2*) upon SARS-CoV-2 infection and a downregulation of lactate dehydrogenase A (*LDHA*) and TP53 induced glycolysis regulatory phosphatase (*TIGAR*) after betamethasone treatment, all of which are involved in the glycolysis and therefore affects HA metabolism (supplementary table 1).

Based on our results, we present a model where the positive action of betamethasone in severe COVID-19 patients is a combined action of a reduced inflammatory response (Figure 5A, supplementary table 1) and a reduction of the pathological overproduction of HA upon SARS-CoV-2 infection (Figure 5B, supplementary table 1).

DISCUSSION

We have previously shown that lungs from deceased COVID-19 patients are filled with a clear liquid jelly consisting of HA, which impairs the capillary-alveolar gas exchange and leads to respiratory failure. In this study, we investigated the mechanisms behind the pathological increase in HA levels to possibly identify new therapeutic targets, using a human *in vitro* 3D-lung model, which showed a SARS-CoV-2-induced inflammatory response, and an increase in HA-production, both of which were counteracted by corticosteroid treatment. Furthermore, we examined blood plasma concentrations of HA in patients with COVID-19 and found an association with disease severity, and importantly, that HA concentrations remained elevated compared to healthy controls for at least 12 weeks after symptom onset.

We showed that despite an overall reduction in HA concentrations during the convalescent phase (≥12 weeks), the levels did not normalize in either mild or severe COVID-19 patients and remained significantly higher compared to the control group. Prior studies have demonstrated an elevation of HA concentration correlating with disease severity in the acute phase of COVID-19 (7, 8), but the long-term consequences of COVID-19 on HA levels have not previously been thoroughly investigated. The tissue half-life of HA ranges from half a day to two-three days, and the half-time in blood is ever shorter (19). The sustained elevation of HA concentrations demonstrated here therefore suggest an imbalance in the production and degradation of HA that remains for at least 12 weeks after disease onset, even after mild disease.

We also found that HA levels were higher in women than in men during the convalescent phase. This is of particular interest in light of previous studies that have identified female sex as a risk factor for developing an impaired diffusion capacity after COVID-19 (20, 21). While female sex hormones appear to protect from severe COVID-19 during the acute phase (22), they might have a negative impact on long-term health consequences (23). Further studies with long-term patient follow up will give the possibility to explore the role of HA on long-term lung function impairment as well as other long-term health sequalae of COVID-19.

The molecular mechanisms behind the observed increase in HA synthesis upon SARS-CoV-2 infection remain to be clarified. Based on the results of this study, we here propose a model in which SARS-CoV-2 infection causes transcriptional changes of genes involved in HA metabolism, which are partially counteracted by corticosteroid treatment. In the human *in vitro* 3D-lung model, SARS-CoV-2 infection causes an upregulation of transcription factors *EGR1* and *EGR2*, which in turn activate the expression of HA synthases *HAS2* and *HAS3*. SARS-CoV-2 infection and subsequent replication also induce an increased glucose metabolism in infected cells (24, 25). A few percent of the glucose molecules are processed through side branches in the glycolysis pathway. This results in production of UDP-N-acetylglucosamine (UDP-GlcNAc) and UDP-glucuronic acid (UDP-GlcUA), the two precursors for HA synthesis. Therefore, HA synthesis is increased as a consequence of an increased glucose flux through glycolysis (26). Another outcome of increased glucose metabolism is a rise in lactate production (27). Lactate can bind to the mitochondrial antiviral-signaling (MAVS) protein, an important activator of IFN-I production in response to viral infections. This interaction not only prevents IFN-I production, but, more importantly, the lactate-MAVS complex activates hexokinase 2 (HK2), which transforms glucose to glucose-6P, the first step in the glycolysis (28). Thus, increased HK2 activity pushes more glucose into the glycolysis, which in turn results in

increased HA synthesis. Besides counteracting the SARS-CoV-2 induced effect on *HAS* and *HYAL*, corticosteroid treatment of the infected 3D-lung model decreased the expression of lactate dehydrogenase A (*LDHA*). This may lead to a decreased production of lactate (that can bind to MAVS) and, consequently, reduced glucose transforming activity of HK2, resulting in lower production of precursors for HA synthesis.

Another effect on glycolysis by corticosteroid treatment of the SARS-CoV-2 infected *in vitro* 3D-lung cultures was downregulation of the *TIGAR* gene. TIGAR inhibits the transformation of fructose-6P to fructose 1,6-P_2, thus inhibiting glycolysis downstream of fructose 6-P, making more substrates available for side branches of the glycolysis, such as HA synthesis (29). Hence, less TIGAR and a subsequent increased flux of glucose through the whole glycolysis would result in less glucose for HA synthesis.

The transcriptional changes induced by SARS-CoV-2 infection described here can all result in increased HA production. It is however possible that additional pathways can affect HA production. It was recently shown that specific RNA sequences in the SARS-CoV-2 genome can activate expression of *HAS2* and, consequently, increase HA synthesis (30).

Today, one of the few evidence-based treatment options for patients with severe to critical COVID-19, presenting after the first week after onset, is corticosteroids (9). However, the timing of treatment seems to be crucial. Early treatment of COVID-19 patients with corticosteroids has been shown to have less positive effect than treating severely ill patients (9). This could result from the strong anti-inflammatory features of corticosteroids, which interfere with an essential immune defense against the virus early in infection, as opposed to later stages of severe COVID-19, where pronounced inflammation of the lungs dominates and the negative effects of corticosteroids may carry less impact. The increased levels of HA in the blood from both mild and severe cases of COVID-19, shown by us and others (7, 8), indicate a dysregulated

HA metabolism in COVID-19. We observed an increase in gene expression of HA synthases and a decrease of degrading hyaluronidases caused by SARS-CoV-2 infection of our lung model. This resulted in a subsequent rise in HA concentration in the apical secretions of the *in vitro* 3D-lung cultures, which confirmed a SARS-CoV-2-related effect on HA metabolism. Hyaluronan production and/or degradation therefore poses an attractive treatment target for severe COVID-19. Hymecromone, an FDA-approved drug for treatment of biliary spasm, has a more direct action against HA synthesis and could be used to specifically treat the overproduction of HA. Such a high-precision treatment could avoid some of the negative effects of corticosteroid and enable treatment at an earlier stage to prevent disease progression. A recent clinical trial with hymecromone showed efficient inhibition of COVID-19 progression and warrants further investigations (31).

In summary, our results showed sustained increased levels of HA in peripheral blood in COVID-19 patients, which could be explained by the mechanisms identified in our *in vitro* lung model including an imbalance in HA production and degradation induced upon SARS-CoV-2 infection. The clinical significance of these findings needs to be further investigated along with the potential effect on long-term health sequalae. The increasing number of reports on elevated HA levels in severe COVID-19 patients, along with our observation that HA concentrations remain high for at least 12 weeks, implicate HA as an important factor in COVID-19 pathogenesis. Studies on targeting HA metabolism as an alternative or complementary treatment to corticosteroids to reduce the acute and long-term health consequences of COVID-19 are warranted.

Acknowledgement:

The authors thank the team at Affinity Proteomics Uppsala, SciLifeLab Sweden, for providing assistance in protein analyzes (Olink data). We acknowledge our study nurses Ida-Lisa Persson and Anna Kauppi at the Department of Infectious Diseases in Umeå and Christine Degner, Anna Segerås and Lena Irvhage in Örebro, and the personnel at the Clinical Research Center at Umeå University Hospital and Örebro University Hospital for enrolment and sampling of study participants. Figure 1 and 5 were created using BioRender.com.

REFERENCES

1. Gavriatopoulou M, Korompoki E, Fotiou D, Ntanasis-Stathopoulos I, Psaltopoulou T, Kastritis E, Terpos E, Dimopoulos MA. Organ-specific manifestations of COVID-19 infection. *Clin Exp Med* 2020; 20: 493-506.
2. Xu Z, Shi L, Wang Y, Zhang J, Huang L, Zhang C, Liu S, Zhao P, Liu H, Zhu L, Tai Y, Bai C, Gao T, Song J, Xia P, Dong J, Zhao J, Wang FS. Pathological findings of COVID-19 associated with acute respiratory distress syndrome. *Lancet Respir Med* 2020; 8: 420-422.
3. Laurent TC, Laurent UB, Fraser JR. The structure and function of hyaluronan: An overview. *Immunol Cell Biol* 1996; 74: A1-7.
4. Hallgren R, Samuelsson T, Laurent TC, Modig J. Accumulation of hyaluronan (hyaluronic acid) in the lung in adult respiratory distress syndrome. *Am Rev Respir Dis* 1989; 139: 682-687.
5. Hellman U, Karlsson MG, Engstrom-Laurent A, Cajander S, Dorofte L, Ahlm C, Laurent C, Blomberg A. Presence of hyaluronan in lung alveoli in severe Covid-19: An opening for new treatment options? *J Biol Chem* 2020; 295: 15418-15422.
6. Kratochvil MJ, Kaber G, Demirdjian S, Cai PC, Burgener EB, Nagy N, Barlow GL, Popescu M, Nicolls MR, Ozawa MG, Regula DP, Pacheco-Navarro AE, Yang S, de Jesus Perez VA, Karmouty-Quintana H, Peters AM, Zhao B, Buja ML, Johnson PY, Vernon RB, Wight TN, Stanford C-BSG, Milla CE, Rogers AJ, Spakowitz AJ, Heilshorn SC, Bollyky PL. Biochemical, biophysical, and immunological characterization of respiratory secretions in severe SARS-CoV-2 infections. *JCI Insight* 2022; 7.
7. Ding M, Zhang Q, Li Q, Wu T, Huang YZ. Correlation analysis of the severity and clinical prognosis of 32 cases of patients with COVID-19. *Respir Med* 2020; 167: 105981.
8. Donlan AN, Sutherland TE, Marie C, Preissner S, Bradley BT, Carpenter RM, Sturek JM, Ma JZ, Moreau GB, Donowitz JR, Buck GA, Serrano MG, Burgess SL, Abhyankar MM, Mura C, Bourne PE, Preissner R, Young MK, Lyons GR, Loomba JJ, Ratcliffe SJ, Poulter MD, Mathers AJ, Day AJ, Mann BJ, Allen JE, Petri WA, Jr. IL-13 is a driver of COVID-19 severity. *JCI Insight* 2021; 6.
9. Group RC, Horby P, Lim WS, Emberson JR, Mafham M, Bell JL, Linsell L, Staplin N, Brightling C, Ustianowski A, Elmahi E, Prudon B, Green C, Felton T, Chadwick D, Rege K, Fegan C, Chappell LC, Faust SN, Jaki T, Jeffery K, Montgomery A, Rowan K, Juszczak E, Baillie JK, Haynes R, Landray MJ. Dexamethasone in Hospitalized Patients with Covid-19. *N Engl J Med* 2021; 384: 693-704.
10. Ernst G, Lompardia S, Cordo Russo R, Gentilini V, Venturiello S, Galindez F, Grynblat P, Hajos SE. Corticosteroid administration reduces the concentration of hyaluronan in bronchoalveolar lavage in a murine model of eosinophilic airway inflammation. *Inflamm Res* 2012; 61: 1309-1317.
11. Engstrom-Laurent A, Hallgren R. Circulating hyaluronate in rheumatoid arthritis: relationship to inflammatory activity and the effect of corticosteroid therapy. *Ann Rheum Dis* 1985; 44: 83-88.
12. Characterisation WHOWGotC, Management of C-i. A minimal common outcome measure set for COVID-19 clinical research. *Lancet Infect Dis* 2020; 20: e192-e197.
13. Roffman CE, Buchanan J, Allison GT. Charlson Comorbidities Index. *J Physiother* 2016; 62: 171.
14. Harris PA, Taylor R, Thielke R, Payne J, Gonzalez N, Conde JG. Research electronic data capture (REDCap)--a metadata-driven methodology and workflow process for providing translational research informatics support. *J Biomed Inform* 2009; 42: 377-381.
15. Harris PA, Taylor R, Minor BL, Elliott V, Fernandez M, O'Neal L, McLeod L, Delacqua G, Delacqua F, Kirby J, Duda SN, Consortium RE. The REDCap consortium: Building an international community of software platform partners. *J Biomed Inform* 2019; 95: 103208.
16. Rosendal E, Mihai IS, Becker M, Das D, Frangsmyr L, Persson BD, Rankin GD, Groning R, Trygg J, Forsell M, Ankarklev J, Blomberg A, Henriksson J, Overby AK, Lenman A. Serine Protease Inhibitors Restrict Host Susceptibility to SARS-CoV-2 Infections. *mBio* 2022: e0089222.
17. Liao Y, Smyth GK, Shi W. featureCounts: an efficient general purpose program for assigning sequence reads to genomic features. *Bioinformatics* 2014; 30: 923-930.

485 18. Love MI, Huber W, Anders S. Moderated estimation of fold change and dispersion for RNA-seq data
486 with DESeq2. *Genome Biol* 2014; 15: 550.
487 19. Fraser JR, Laurent TC, Laurent UB. Hyaluronan: its nature, distribution, functions and turnover. *J*
488 *Intern Med* 1997; 242: 27-33.
489 20. Wu X, Liu X, Zhou Y, Yu H, Li R, Zhan Q, Ni F, Fang S, Lu Y, Ding X, Liu H, Ewing RM, Jones MG, Hu Y,
490 Nie H, Wang Y. 3-month, 6-month, 9-month, and 12-month respiratory outcomes in patients
491 following COVID-19-related hospitalisation: a prospective study. *Lancet Respir Med* 2021; 9:
492 747-754.
493 21. Huang L, Yao Q, Gu X, Wang Q, Ren L, Wang Y, Hu P, Guo L, Liu M, Xu J, Zhang X, Qu Y, Fan Y, Li X,
494 Li C, Yu T, Xia J, Wei M, Chen L, Li Y, Xiao F, Liu D, Wang J, Wang X, Cao B. 1-year outcomes in
495 hospital survivors with COVID-19: a longitudinal cohort study. *Lancet* 2021; 398: 747-758.
496 22. Sund M, Fonseca-Rodriguez O, Josefsson A, Welen K, Fors Connolly AM. Association between
497 pharmaceutical modulation of oestrogen in postmenopausal women in Sweden and death due
498 to COVID-19: a cohort study. *BMJ Open* 2022; 12: e053032.
499 23. Stewart S, Newson L, Briggs TA, Grammatopoulos D, Young L, Gill P. Long COVID risk - a signal to
500 address sex hormones and women's health. *Lancet Reg Health Eur* 2021; 11: 100242.
501 24. Codo AC, Davanzo GG, Monteiro LB, de Souza GF, Muraro SP, Virgilio-da-Silva JV, Prodonoff JS,
502 Carregari VC, de Biagi Junior CAO, Crunfli F, Jimenez Restrepo JL, Vendramini PH, Reis-de-
503 Oliveira G, Bispo Dos Santos K, Toledo-Teixeira DA, Parise PL, Martini MC, Marques RE, Carmo
504 HR, Borin A, Coimbra LD, Boldrini VO, Brunetti NS, Vieira AS, Mansour E, Ulaf RG, Bernardes
505 AF, Nunes TA, Ribeiro LC, Palma AC, Agrela MV, Moretti ML, Sposito AC, Pereira FB, Velloso LA,
506 Vinolo MAR, Damasio A, Proenca-Modena JL, Carvalho RF, Mori MA, Martins-de-Souza D,
507 Nakaya HI, Farias AS, Moraes-Vieira PM. Elevated Glucose Levels Favor SARS-CoV-2 Infection
508 and Monocyte Response through a HIF-1alpha/Glycolysis-Dependent Axis. *Cell Metab* 2020;
509 32: 437-446 e435.
510 25. Laviada-Molina HA, Leal-Berumen I, Rodriguez-Ayala E, Bastarrachea RA. Working Hypothesis for
511 Glucose Metabolism and SARS-CoV-2 Replication: Interplay Between the Hexosamine Pathway
512 and Interferon RF5 Triggering Hyperinflammation. Role of BCG Vaccine? *Front Endocrinol*
513 *(Lausanne)* 2020; 11: 514.
514 26. Hascall VC, Wang A, Tammi M, Oikari S, Tammi R, Passi A, Vigetti D, Hanson RW, Hart GW. The
515 dynamic metabolism of hyaluronan regulates the cytosolic concentration of UDP-GlcNAc.
516 *Matrix Biol* 2014; 35: 14-17.
517 27. Munger J, Bennett BD, Parikh A, Feng XJ, McArdle J, Rabitz HA, Shenk T, Rabinowitz JD. Systems-
518 level metabolic flux profiling identifies fatty acid synthesis as a target for antiviral therapy. *Nat*
519 *Biotechnol* 2008; 26: 1179-1186.
520 28. Zhang W, Wang G, Xu ZG, Tu H, Hu F, Dai J, Chang Y, Chen Y, Lu Y, Zeng H, Cai Z, Han F, Xu C, Jin G,
521 Sun L, Pan BS, Lai SW, Hsu CC, Xu J, Chen ZZ, Li HY, Seth P, Hu J, Zhang X, Li H, Lin HK. Lactate
522 Is a Natural Suppressor of RLR Signaling by Targeting MAVS. *Cell* 2019; 178: 176-189 e115.
523 29. Tang J, Chen L, Qin ZH, Sheng R. Structure, regulation, and biological functions of TIGAR and its role
524 in diseases. *Acta Pharmacol Sin* 2021; 42: 1547-1555.
525 30. Li W, Yang S, Xu P, Zhang D, Tong Y, Chen L, Jia B, Li A, Lian C, Ru D, Zhang B, Liu M, Chen C, Fu W,
526 Yuan S, Gu C, Wang L, Li W, Liang Y, Yang Z, Ren X, Wang S, Zhang X, Song Y, Xie Y, Lu H, Xu J,
527 Wang H, Yu W. SARS-CoV-2 RNA elements share human sequence identity and upregulate
528 hyaluronan via NamiRNA-enhancer network. *EBioMedicine* 2022; 76: 103861.
529 31. Yang S, Ling Y, Zhao F, Li W, Song Z, Wang L, Li Q, Liu M, Tong Y, Chen L, Ru D, Zhang T, Zhou K,
530 Zhang B, Xu P, Yang Z, Li W, Song Y, Xu J, Zhu T, Shan F, Yu W, Lu H. Hymecromone: a clinical
531 prescription hyaluronan inhibitor for efficiently blocking COVID-19 progression. *Signal*
532 *Transduct Target Ther* 2022; 7: 91.

533

FIGURES

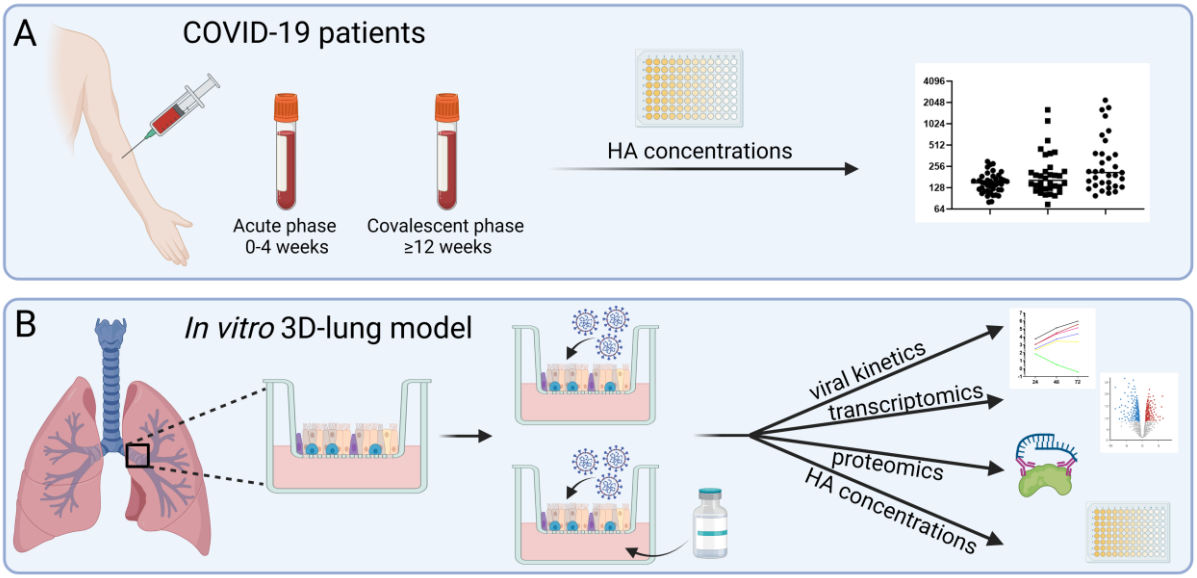

Figure 1. Schematic presentation of study outline. A) Blood samples were collected from COVID-19 patients during the acute phase and convalescent phase of the disease. Hyaluronan concentrations were determined by ELISA. B) A primary 3D-lung model was established and infected with SARS-CoV-2 in the presence or absence of corticosteroids to investigate the effect on inflammation and hyaluronan metabolism.

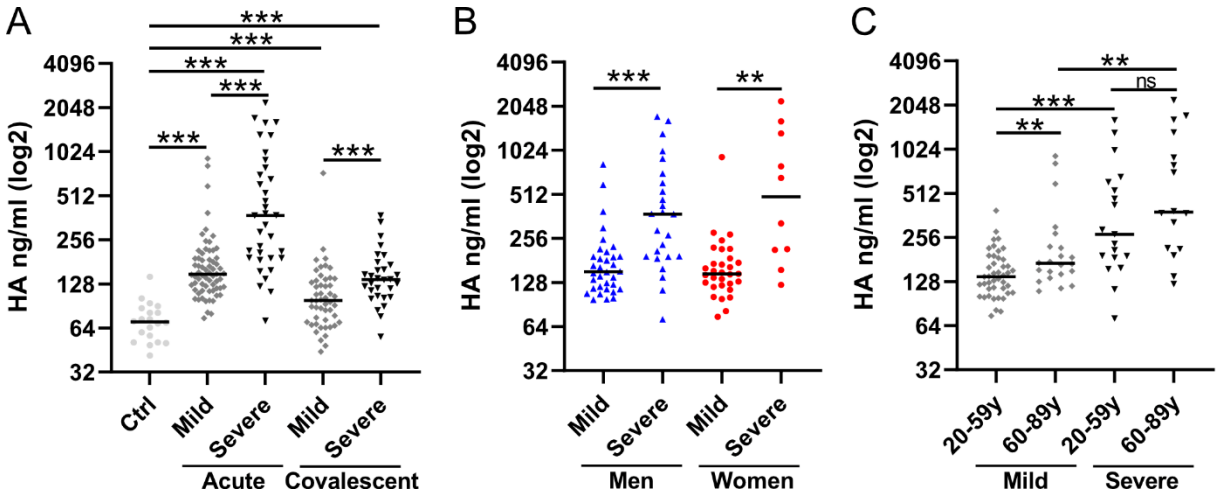

Figure 2. Hyaluronan (HA) plasma concentrations are elevated in COVID-19 patients and associated with disease severity. A) HA concentrations in patients with severe and mild COVID-19 compared to controls (Ctrl). Samples were taken during the acute phase (0-4 weeks from disease onset) and again at least 12 weeks after disease onset (convalescent phase). **B-C)** HA concentrations in plasma during the acute phase grouped on severity and **B)** sex or **C)** age. Each dot represents one patient and the line represents the median. Severity was based on WHO Clinical Progression Scale (WHO-CPS) with patients requiring high-flow nasal oxygen treatment and/or admission to the intensive care unit during the acute phase of illness classified as "severe", corresponding to WHO-CPS 6-9, and all other patients as "mild", WHO-CPS 1-5. Statistical significance was calculated by Mann-Whitney U test (*$p < 0.05$, **$p < 0.01$, ***$p < 0.001$).

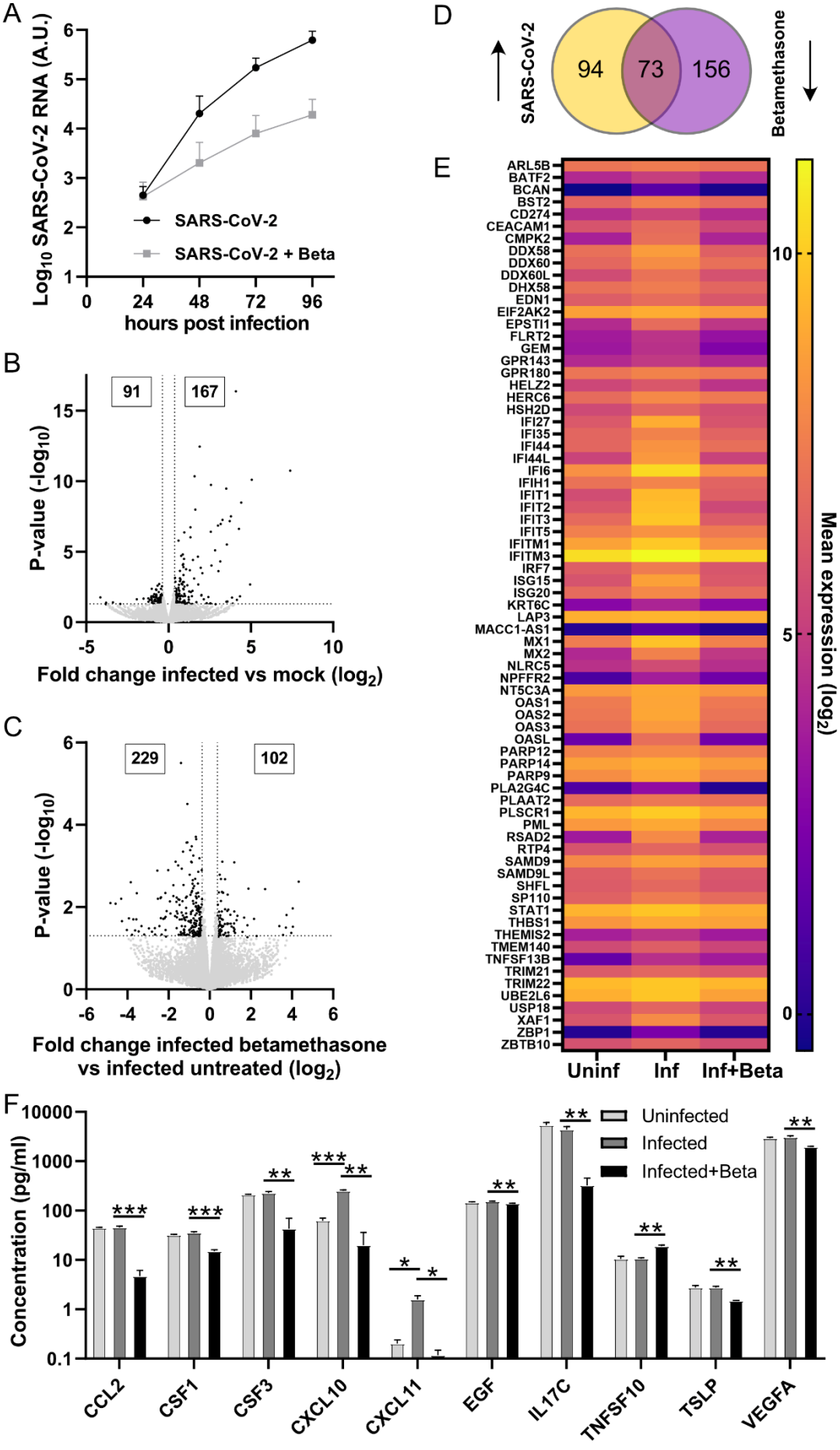
A
Log10 SARS-CoV-2 RNA (A.U.)
hours post infection
SARS-CoV-2
SARS-CoV-2 + Beta
B
91
167
P-value (-log10)
Fold change infected vs mock (log2)
C
229
102
P-value (-log10)
Fold change infected betamethasone vs infected untreated (log2)
D
SARS-CoV-2
94
73
156
Betamethasone
E
Mean expression (log2)
Uninf
Inf
Inf+Beta
F
Concentration (pg/ml)
Uninfected
Infected
Infected+Beta
CCL2
CSF1
CSF3
CXCL10
CXCL11
EGF
IL17C
TNFSF10
TSLP
VEGFA

556

Figure 3. Inflammatory response and effect of corticosteroid treatment in a SARS-CoV-2 infected 3D-lung model. A) The lung cultures based on differentiated primary human bronchial epithelial cells at an air-liquid interface were pretreated with/without betamethasone (Beta) in the basal media for 20 h prior to infection with SARS-CoV-2 (multiplicity of infection= 0.5). The accumulated viral release from the apical side of the cultures was quantified by qPCR at indicated timepoints. **B-C)** Volcano plot showing differentially expressed genes between **B)** infected vs uninfected (mock) lung cultures and **C)** infected lung cultures with betamethasone vs without betamethasone treatment. The statistical *p*-value ($-\log_{10}$) is plotted against the fold change in gene expression ($\log_2$). Dotted lines highlight the significance cut off corresponding to a fold change of 1.3 and p-value=0.05. **D)** Venn diagram showing the overlap between the genes significantly upregulated upon SARS-CoV-2 infection compared to genes downregulated by betamethasone treatment. **E)** Heatmap displaying the mean expression ($\log_2$) of the overlapping genes from the Venn diagram in uninfected, infected and infected + betamethasone-treated lung cultures. **F)** Cytokine levels in basolateral samples from HBEC ALI-cultures collected at 96 h post infection analyzed by Proximity Extension Assay (Olink). Mean values and SEM are shown, statistical significance was calculated by unpaired t-test (*$p < 0.05$, **$p < 0.01$***$p < 0.001$).

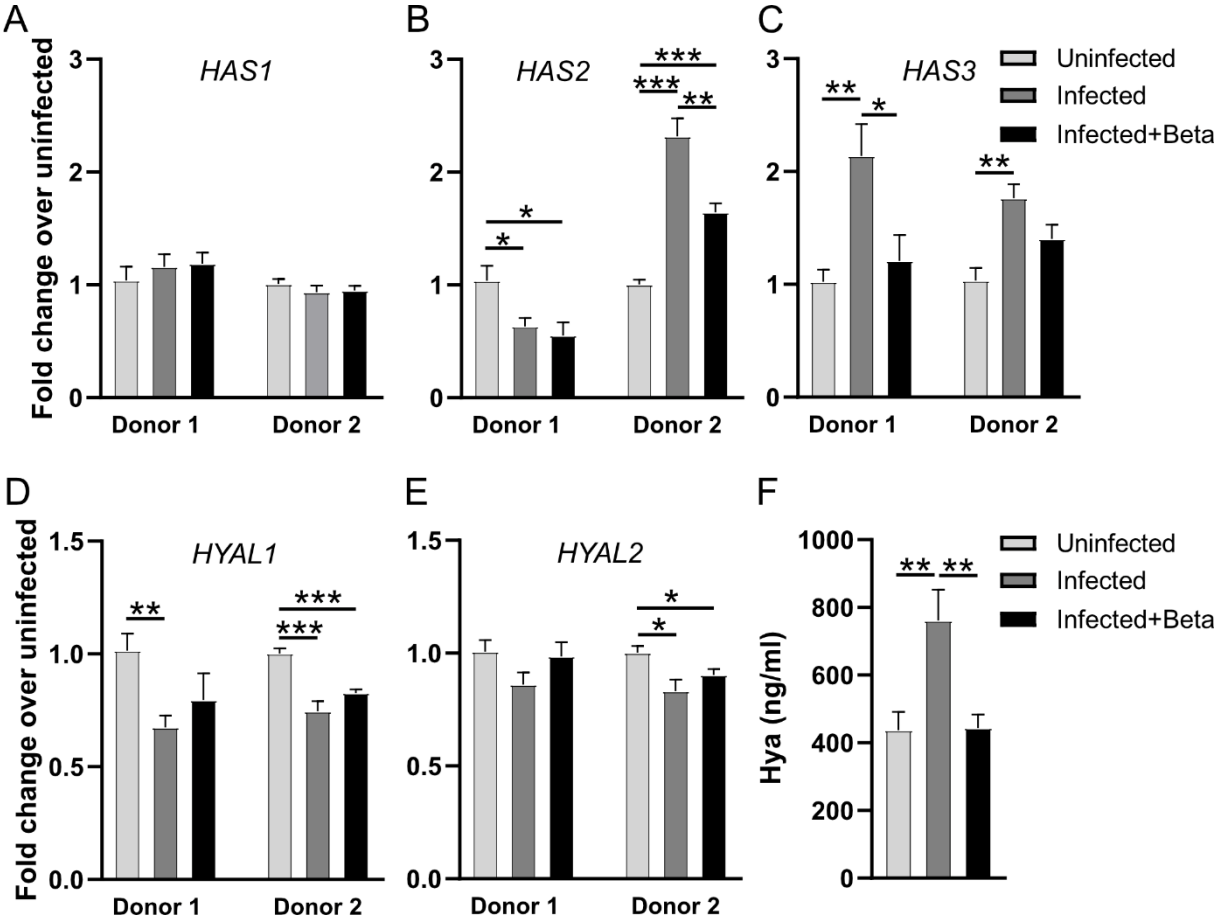

Figure 4. SARS-CoV-2 increases hyaluronan (HA) concentrations in a 3D-lung model by upregulation of HA synthases and downregulation of hyaluronidases, which is partly counteracted by corticosteroid treatment. The gene expression levels of HA synthases **A)** *HAS1*, **B)** *HAS2* and **C)** *HAS3* along with the hyaluronidases **D)** *HYAL1* and **E)** *HYAL2* were determined by qPCR 120 h post SARS-CoV-2 infection of lung cultures from two different donors. **F)** HA concentrations were determined by ELISA in apical secretions from lung cultures 120 h post infection. Mean values and SEM are shown, statistical significance was calculated by unpaired t-test (*$p < 0.05$, **$p < 0.01$***$p < 0.001$).

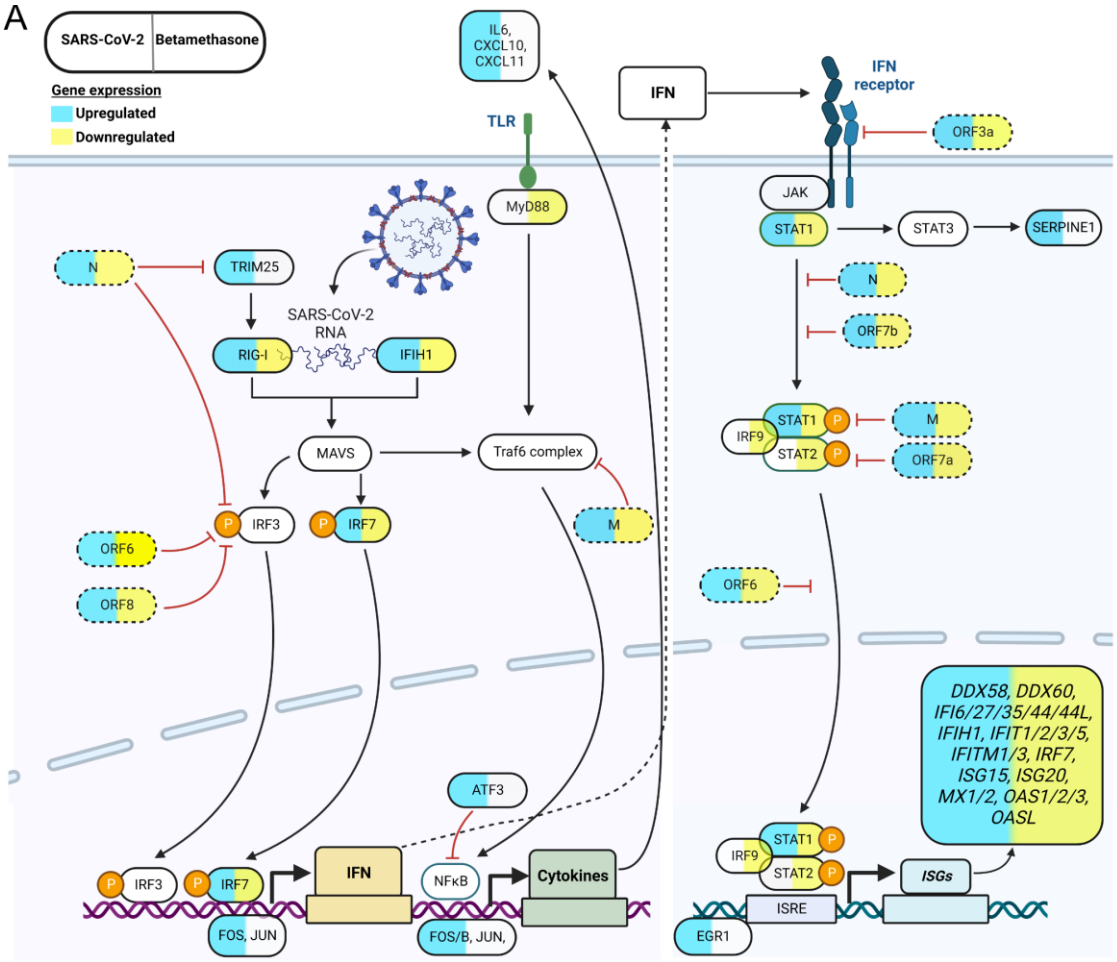
A
SARS-CoV-2
Betamethasone
Gene expression
Upregulated
Downregulated
IL6, CXCL10, CXCL11
TLR
MyD88
IFN
IFN receptor
ORF3a
JAK
STAT1
STAT3
SERPINE1
N
ORF7b
N
TRIM25
SARS-CoV-2 RNA
RIG-I
IFIH1
MAVS
Traf6 complex
IRF9
STAT1
STAT2
M
ORF7a
IRF3
IRF7
M
ORF6
ORF8
ORF6
DDX58, DDX60, IFI6/27/35/44/44L, IFIH1, IFIT1/2/3/5, IFITM1/3, IRF7, ISG15, ISG20, MX1/2, OAS1/2/3, OASL
ATF3
IFN
NFκB
Cytokines
ISGs
ISRE
EGR1
FOS, JUN
FOS/B, JUN,

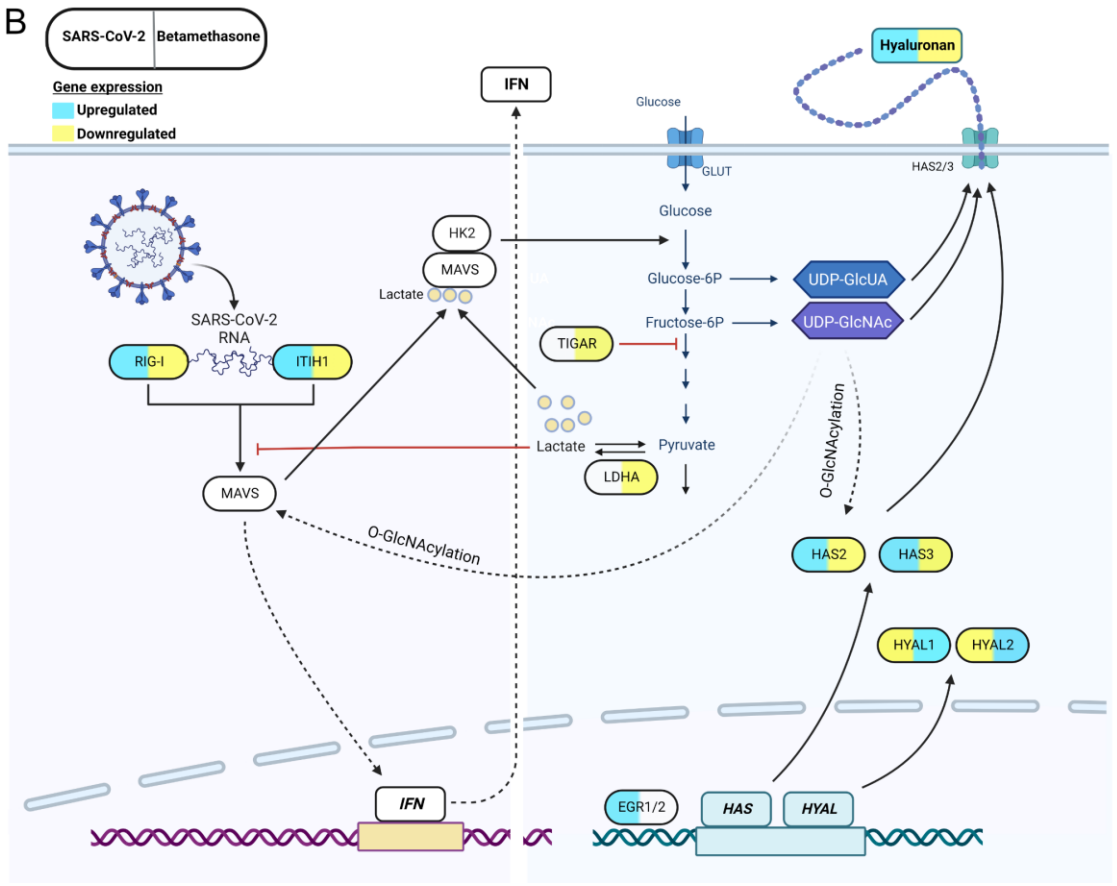
B
SARS-CoV-2
Betamethasone
Gene expression
Upregulated
Downregulated
IFN
Hyaluronan
Glucose
GLUT
HAS2/3
Glucose
HK2
MAVS
Lactate
Glucose-6P
UDP-GlcUA
Fructose-6P
UDP-GlcNAc
TIGAR
SARS-CoV-2 RNA
RIG-I
ITIH1
Lactate
Pyruvate
LDHA
O-GlcNAcylation
MAVS
O-GlcNAcylation
HAS2
HAS3
HYAL1
HYAL2
IFN
EGR1/2
HAS
HYAL

593

Figure 5. The effect of SARS-CoV-2 and betamethasone on cellular pathways regulating IFN-I responses and hyaluronan (HA) production in a human *in vitro* 3D-lung model. Schematic presentation of a cell infected with SARS-CoV-2 with or without betamethasone treatment and affected cellular pathways regulating **A)** the IFN-I response and **B)** HA production. Left side of the gene shows effect on gene expression upon SARS-CoV-2 infection, and right side shows effect of betamethasone treatment in infected lung cultures. Blue color corresponds to an increase in gene expression and yellow indicates a decrease in gene expression. Viral genes are represented by dotted lines.

TABLES

Table 1. Demography and characteristics of COVID-19 patients.

Patient characteristics	Mild (n = 66)	Severe (n = 37)	p-value
Demography			
Age years (range)	54.5 (25-81)	58.0 (21-82)	0.584
Women N (%)	31 (47.0)	11 (29.7)	0.112
BMI	26.3 (19.2-48.4)	30.5 (18.6-47.4)	<0.001
Comorbidities			
Diabetes N (%)	5 (7.6)	4 (10.8)	0.719
Hypertension N (%)	17 (25.8)	12 (32.4)	0.500
Cardiovascular disease[a] N (%)	11 (16.7)	4 (10.8)	0.564
Chronic pulmonary disease[b] N (%)	11 (16.7)	8 (21.6)	0.600
Autoimmune disease N (%)	5 (7.6)	2 (5.4)	1.000
Charlson comorbidity index	0 (0-4)	0 (0-7)	0.584
Laboratory findings			
C-reactive protein, max (mg/L)[c]	12 (0.7-262)	166 (4-623)	<0.001
Hemoglobin, min g/L[d]	134 (96-152)	126 (72-151)	0.004
White blood cell count, max (10e9/L)[d]	6.9 (2.8-17.6)	11.9 (4.9-41.1)	<0.001
Neutrophil count, max (10e9/L)[d]	4.15 (1.3-13.6)	9.3 (3.0-31.4)	<0.001
Lymphocyte count, max (10e9/L)[d]	2.05 (0.8-3.9)	2.3 (0.6-35.0)	0.061
Platelet count, min (10e9/L)[e]	193 (102-409)	187 (49-345)	0.251
P-Creatinine, max (µmol/L)[d]	77.5 (53-174)	79 (38-295)	0.975
Interleukin-6 max (ng/L)[f]	22 (2-205)	141 (2-1661)	0.002

Descriptive data of the patient cohort. All values presented as median and range if not otherwise stated.

Differences between groups analyzed by Mann-Whitney U-test (continuous variables) and Fisher's exact test (dichotomous variables). No correction for multiple testing was performed.

[a]Including: Heart failure, ischemic heart disease, peripheral arterial insufficiency, deep venous thrombosis, and pulmonary embolism.

[b]Including: Asthma and chronic obstructive pulmonary disease.

[c]N=91, [d]N=93, [e]N=92, [f]N=66